CONTINUOUS BEAM STEERING FROM A SEGMENTED LIQUID CRYSTAL OPTICAL PHASED ARRAY

Charles M. Titus

Liquid Crystal Institute

Kent State University, Kent, OH 44242

John Pouch, Hung Nguyen, Félix Miranda

NASA Glenn Research Center

21000 Brookpark Road

Cleveland, OH 44135

Philip J. Bos

Liquid Crystal Institute

Kent State University, Kent, OH 44242

Abstract

Optical communications to and from deep space probes will require beams possessing divergence on the order of a microradian, and must be steered with sub-microradian precision. Segmented liquid crystal spatial phase modulators, a type of optical phased array, are considered for this ultra-high resolution beam steering. It is shown here that in an ideal device of this type, there are ultimately no restrictions on the angular resolution. Computer simulations are used to obtain that result, and to analyze the influence of beam truncation and substrate flatness on the performance of this type of device.

1. Introduction

As NASA develops a need to transmit greater amounts of data over long distances, there is a need to develop new technologies capable of such performance[1,2]. Current S- and X-band RF technology provides only limited room for increasing the data communication rate[2,3]. The use of Ka-band technology may increase the usable photon flux by a few orders of magnitude, but even that may not be enough to permit, for example, high-speed long-distance communication of high-resolution image data[4]. In addition, increasing the RF transmitter power level does not get past bandwidth limitations of the carrier frequency. For that reason, NASA is exploring the use of shorter wavelengths in the near IR, where the greater directivity of transmitting beams can increase photon flux and bandwidth.

However, this potential benefit is not without cost, for it involves trading problems with existing RF technology for a new set of problems. Among these new problems is the necessity for some means of high-resolution optical beam steering in order to maintain connection of the more directional signal beam with the distant receiver. Because of the anticipated demand for higher data rates at all transmission distances, special steps must be taken in order to ensure a high signal concentration at the receiving end. In order to maintain the intensity of a propagating laser beam after long propagation distances, the beam must possess a divergence of a few microradians or less. Along with this directivity requirement comes the need for steering capability of even greater accuracy, i.e. sub-microradian beam pointing technology[5].

The most mature beam steering devices achieve deflection through mechanical means. Although mechanical pointing technology is being considered for use in deep-space optical communications[5,6,7], such devices may not provide the needed precision.

In this paper we discuss factors influencing the range, resolution, and number of steering angles available from a liquid crystal spatial phase modulator (LC-SPM). Computational simulations are used to quantify the effect of phase stair-stepping on beam steering (i.e. diffractive) performance. Simulation data is also presented to quantify the impact of beam truncation by the diffracting aperture and surface flatness.

These devices can be designed at or between either of two extremes; large pixels producing stair-stepped phase modulation or small pixels whose director distortions produce smoothed phase profiles. Here, we discuss the large pixel variety. The effects of director distortion and finite cell thickness will be considered in later publications

2. Background

The LC-SPM consists of two glass plates sandwiching a thin (~10μm or less) layer of liquid crystalline material. One substrate is coated with a single common electrode, usually held at zero Volts. The other glass substrate is patterned with a number of uniformly sized and spaced discrete electrodes.

If suitably addressed, the electrodes of the LC-SPM selectively reorient the liquid crystal to form a one-dimensional phase grating. That grating is used to impose a periodic "blazed" phase profile onto incident light (Fig 1). The goal is to provide the equivalent of a linear phase ramp with its 2π phase degeneracies removed (Fig. 2). Operated in this fashion, the LC-SPM can be used as a means of redirecting the path of monochromatic light in one dimension. Two-dimensional beam steering can be obtained by either cascading two one-dimensional LC-SPM's, or possibly by encoding onto a single device a two-dimensional array of individually addressable electrodes.

The use of an LC-SPM in this manner has carried the label of Optical Phased Array (OPA) technology[8,9]. In one implementation of liquid crystal OPA technology[10], every n^{th} electrode is linked together in order to reduce the number of off-device connections. That approach is taken primarily to make more practical the fabrication of large apertures containing a large number of electrodes. However, that approach also limits available steering angles to a discrete number of angularly separated deflections. In order to completely cover an entire region of interest, cascading with a second fine-tuning stage is required. Technology does exist for connecting and *individually* addressing each of a moderately large number of (more than one thousand) electrodes. This latter form of LC-OPA technology is the subject of this paper.

Prior analysis of the OPA, for which identical stair-stepped phase approximations of ideal blaze periods are repeated across the entire device, has yielded a theoretical maximum beam steering efficiency of[8]:

$$\eta = \mathrm{sinc}^2(\pi / N) \tag{1}$$

where N is the number of stair-stepped phase segments in each identical blaze profile. It is assumed that all modulo-2π resets of the original ideal phase profile fall between electrodes. Below we will show this result extends to the more general case of resets falling anywhere in the LC-SPM, even in the middle of electrodes, if the phase retardation produced by those electrodes is properly chosen. Hence, it is predicted that individually addressable lines will permit continuous steering from this stair-stepped LC-SPM device, without any efficiency penalty beyond that imposed by Eq. (1). In other words, this device does not, in theory, possess any pixel-related limit to angular resolution. This potential for achieving continuous steering from liquid crystal OPA technology has not, to our knowledge, been previously analyzed and discussed.

Experimental measurement of the beam steering efficiency of one OPA-like liquid crystal grating was shown to fall short of that predicted by Eq. (1)[11]. The cause of that discrepancy is one of the motivations for this paper.

As was mentioned, these devices can be implemented at or between two extremes. At one extreme the LC-SPM pixels or stripes (one for each electrode) consist of electrodes large enough that the phase profile exhibits stair-stepping. Fringe fields and liquid crystal elasticity at the edges of electrodes (i.e. at the boundaries between adjacent pixels or stripes) cause some smoothing of this stair-stepping, but the area occupied by those behaviors is relatively insignificant relative to the much larger area of the electrodes as a whole. As a result, the device exhibits relatively sharp phase "resets", closely approximating that of an "ideal" blazed phase grating (Fig. 3a). At the other extreme, the pixels or stripes would be small enough that fringe fields and liquid crystal elasticity completely smooth out the phase profile, preventing the appearance of sharp phase "resets" (Fig. 3b). This paper will be restricted to the former extreme.

3. Methodology

Assuming the thin-layer model, diffractive behavior can be obtained by means of Fourier analysis or by numerical evaluation of an appropriate scalar diffraction integral, such as the Integral Theorem of Helmholtz and Kirchhoff[12]:

$$\psi(\mathbf{r}) = \frac{1}{4\pi} \iint_{S'} \mathbf{n} \bullet \left[\psi(\mathbf{r}') \nabla' G - G \nabla' \psi(\mathbf{r}') \right] dS' \qquad (2)$$

where ψ is a complex scalar field, $\mathbf{r}'=(x',y',z')$ is a location on the exit surface S' of the diffracting object, $\mathbf{r}=(x,y,z)$ is a location of some diffraction observation, $\boldsymbol{n}$ is the local normal to the surface of the diffracting object, and G is the appropriate Green's function. For a one-

dimensional grating such as is central to this discussion, the above equation is easily recast as a line integral[13]:

$$\psi(\mathbf{r}) = -\frac{\exp\left(-i\pi/4\right)}{(8k\pi)^{1/2}} \int_{-d}^{d} \frac{\exp(ikR_{\|})}{R_{\|}^{1/2}} \left[\partial_y \psi(x') + \frac{iky}{R_{\|}} \psi(x') \right] dx' \tag{3}$$

where for a one-dimensional planar diffracting aperture $R_{\|}=|\mathbf{r}-\mathbf{r}'|$, $\mathbf{r}=(x,y,0)$, $\mathbf{r}'=(x',0,0)$, k is the magnitude of the wave vector, and the aperture extends over the range $x\subset[-d,d]$.

The two terms inside the bracket in Eq. (3) are direct descendants of the two Rayleigh-Sommerfeld components of Eq. (2). In general, if paraxial calculations are carried out for feature sizes within the aperture and propagation distance both much larger than the wavelength, the two Rayleigh-Sommerfeld components and the Helmholtz-Kirchhoff average of the two do not produce significantly different results, in particular for small deflection angles. The computations in this study evaluate the second term. For a Gaussian profile at the minimum beam waist, that term is the one-dimensional profile of the electric field of the beam:

$$\psi(x') = E_0 \exp\left[-(x')^2 / w_0^2 \right] \exp[i\phi(x')] \tag{4}$$

where w_0 is the minimum beam waist radius and x' is the in-plane distance from the center of the beam. In order to simulate phase gratings, the phase term, $\exp[i\phi(x')]$ can be tailored to the desired grating profile. For an unhindered Gaussian beam, $\phi(x)=0$. This scalar form of the phase-modulated source constitutes a thin layer approximation of fields transmitted through the grating.

Since the application of interest is optical communication to and from deep space probes, it is assumed that the propagation distance $R_{\|}=|\mathbf{r}-\mathbf{r}'|$ in Eq. (3) is large enough to qualify the

diffractive behavior as "far field" (beyond some propagation distance, angular dependence of diffraction will be independent of that distance).

All calculations below were performed for a λ=1μm Gaussian beam with a minimum waist of 25cm coinciding with the "very thin" LC-SPM. Some results are presented in the form of Strehl ratios. The Strehl ratio is defined here as the ratio of a particular diffracted intensity (field squared) to the peak intensity at the same propagation distance for an unhindered beam. That reference point was computed using the same Gaussian source, for an aperture diameter equal to $8w_0$. For calculations of the Strehl ratio, in which one intensity is divided by another, the value of E_0 is not important.

The calculations below cover small deflection angles and large diffraction distances, so the Fraunhofer approximation could provide enough accuracy. Nevertheless, we have employed the more time consuming but also more accurate method of Eq. (3). The more intuitive Fourier-optics representation (i.e. analytical representation of the Fraunhofer approximation) is not so easily obtained for complicated forms of surface fields, but is given in Appendix A for one of the particular cases appearing in this paper.

4. Results

The above calculation method was utilized to gauge the impact of beam truncation, surface flatness, and phase stair-stepping on the performance of large-pixel LC-SPM's. Since it is desirable to provide the maximum signal intensity to the receiver, it is important to know how each of these factors will influence the design of free-space optical communication components such as the beam-steering LC-SPM.

A. Beam Truncation

It is well known that if an aperture is smaller that the beam of light directed at it, the aperture not only blocks some of the incident light but also redirects some of the transmitted light into higher diffraction orders. This will also affect the Strehl ratio at the center of the propagating beam. For example, the impact of beam truncation on a 25cm-waist beam with λ=1μm is illustrated in Fig. 4. If the aperture's width is four times the minimum beam waist (which is assumed to occur in the aperture "plane"), the Strehl ratio measured at the center of the propagating beam in the far field is still a healthy 0.99. If the aperture size is reduced to three times the minimum waist, the Strehl ratio is reduced to 0.94, and if the aperture is further reduced to twice the minimum waist, to 0.72. Such losses would set an upper limit for the performance of the entire communications system.

B. Imperfect Optical Surfaces

If an optical surface in a beam steering device is less than perfect, those aberrations also reduce the amount of energy delivered to the intended direction. Optical surface imperfections are commonly decomposed into constituent aberration modes, which are then related to image-related effects. Liquid crystal devices employ flat glass and reflective substrates whose surfaces are perhaps better represented as a Fourier sum of surface undulation terms, each term of a different spatial frequency. One can then analyze the optical effect of each frequency component and determine which spatial frequency components, and how much of each, can be tolerated. The basic form of the phase undulation, concave at the center of the one-dimensional slice through the aperture, was given the form:

$$\phi(x) = 2\pi A \cos\left[2\pi\left(\frac{x - x_{midpoint}}{D} - 0.5\right)\right] \tag{5}$$

where A is one-half of the peak-to-valley amplitude of the undulation, x is the surface location, $x_{midpoint}$ is the center of the aperture, and D is the width of the aperture. This factor was substituted into Eq. (4) to obtain the thin-layer approximation of the field transmitted through or reflected from the surface. In the case of a reflected surface, Eq. (5) was multiplied by two, accounting for the total optical path offset.

That effect can be computed for the case of light reflected from a nominally flat mirror. Assuming that the mirror size is four times the minimum waist (which coincides with the mirror surface), the effect of a surface undulation whose period equals the aperture size can be seen in Fig. 5. Those results were obtained for the case of an undulation centered on the mirror, concave at the center. Even if the peak-to-valley undulation amplitude is a very fine $\lambda/20$, the resulting Strehl ratio at the center of the far field is reduced to 0.94. Performance for larger undulation amplitudes is noticeably worse (Fig. 6). For even higher undulation frequencies, light will continue to be diverted into other diffraction orders until the undulations become smaller than a wavelength, at which point the surface will again appear to be flat.

Of course, a glass or reflective silicon substrate employed in a LC-SPM could possess a range of undulation frequencies resulting from the manufacturing process, so no one spatial frequency will dominate. Nevertheless, it is clear that manufacturing imperfections will play a role and should be considered.

There is another reason why this last point provides reason for concern. If space probes are to be equipped with meter-class optical apertures, it will not likely be feasible to launch glass apertures of thickness sufficient to provide stable, precise optical surfaces. Instead, optical

components will likely be of lower mass, and thus not as rigid, more prone to significant surface imperfections. In order to make use of optical surfaces with substantial imperfections, it may be necessary to perform wavefront correction close to the source of the imperfections. It is not inconceivable that a two-dimensional LC-SPM could provide that function while simultaneously steering the beam.

C. Phase Stair-stepping

We now return to the issue of phase stair-stepping, which is the product of the segmented design of LC-SPM electrodes. As shown in Figs. 2 and 3a, the principle behind OPA technology involves removing the 2π degeneracies from a linear phase ramp prescribing the beam deflection angle, and then utilizing that blazed phase profile to assign phase values to the OPA's segments. This process is simple and straightforward if all of the "resets" fall between segments, as shown in Fig. 3a. However, as was mentioned earlier, that approach only permits a finite number of discrete deflection angles, thereby placing a limitation on beam steering *angular resolution.*

The angular resolution, as the term is used here, is not the same as the ability of a beam steering device to resolve spots. The maximum number of resolvable spots obtainable from a beam deflecting device has been defined as the device's maximum deflection angle divided by the beam's "diffraction limited angle"[14]. For a Gaussian beam that angle is defined as the divergence angle. If a beam steering device is engineered to provide deflection to only those separated angles, it will not be capable of continuously covering each point in its angular range with a signal of uniform intensity (see Fig. 7). A device may be capable of resolving the maximum number of spots within its angular range, but unless it can steer to angles between the locations of those spots, its angular resolution is limited to the angle between those spots. In

order to permit very high signal intensities everywhere within the device's angular range, it needs an angular resolution finer than that spot resolution.

Achieving sub-spot angular resolution (i.e. sub-microradian resolution, for deep space optical communications using meter-class transmitting apertures) may at times require that the original linear phase ramp will not produce resets which fall between OPA segments (Fig. 8). It is important that any such OPA segments produce the appropriate phase retardation level. If the phase of those segments is incorrectly assigned, diffraction performance (i.e. beam steering efficiency) will suffer.

One obvious approach is to assign to each of these "interperiod" segments a phase equal to the average value of the ideal blazed phase profile within the segment, as shown in Fig. 9. This approach can then be described as applying two operations to the original linear phase ramp, namely modulo-2π and area averaging, in that order. Those two operations can be reversed, producing interperiod phase values as shown in Fig. 10.

In either case, the resulting phase profile does not, at first glance, appear to form an efficient grating. For instance, applying the first approach to a linear phase ramp for which the modulo-2π blaze width is equal to the width of 2 and 1/3 electrode segments, the resulting phase profile will appear as shown in Fig. 11a. The phase profile using the second approach appears in Fig. 11b. It is only when the blaze width equals an integer number of electrode segments that the stair-stepped phase profile obtained using either approach will produce identical stair-stepped blazes as are found in Fig. 3a.

Diffraction simulations were performed for each of the two gratings. In each simulation, stair-step segments of 100μm were used to define the stair-stepped phase profiles covering a 1m wide one-dimensional aperture. Each simulation was carried out over a range of deflection

angles, each of which is characterized by its own ideal linear phase ramp. Each linear phase ramp corresponds to a number of electrode segments per ideal blaze period, not necessarily an integer. At each value of electrodes per period, the diffracted intensity at the intended far field deflection angle was divided by that produced by the corresponding unbroken linear phase ramp to produce the Strehl ratio data appearing in Fig. 12.

For both stair-step approaches, the Strehl ratio at integer values of electrodes per period matches that obtained from Eq. (1). For non-integer values, the first approach falls well below those values, while the second approach does not. This simulation indicates that continuous, high-resolution steering is possible from the LC-SPM, enough to obtain the sub-microradian precision capable of maintaining signal intensity at a distant receiver. Performance does begin to falter at and below eight electrodes per period, as has been noted[8,11].

Although it might appear that the "irregular periodicity" (see Fig. 11b) of the more desirable second stair-step approach might violate the grating condition of its underlying blazed phase profile, such is not the case. The center of each of the stair-step segments does fall on the underlying linear phase ramp, an on its blazed-phase equivalent.

5. Conclusions

Implementation of optical communications with deep space probes will require very precise sub-microradian steering of the communication beam. We have analyzed the possibility of using liquid crystal spatial phase modulators (LC-SPM) to meet this need. Three factors influencing the beam steering performance of these segmented liquid crystal devices have been analyzed: beam truncation, surface flatness, and phase stair-stepping.

If transmitting a laser beam through an aperture, any truncation of the beam by the aperture detracts from the intensity arriving at a distant receiver. This effect begins to be noticed for apertures less than four times the waist of the beam passing through the aperture.

It is also important to avoid wavefront distortions resulting from imperfect optical surfaces, such as reflective or transmissive substrates used in the fabrication of the LC-SPM. Analysis shows that imperfections of as little as $\lambda/20$ can impose performance penalties of approximately 5%, and much more as the magnitude of surface imperfection grows. If those imperfections cannot be eliminated, wavefront correction is necessary, and the LC-SPM may be capable of performing those corrections.

Further analysis was conducted for one limiting case of LC-SPM, that is electrodes large enough that fringe fields and elastic behavior contribute very little to device performance. In that case, the phase retardation profile produced by an LC-SPM will appear to be stair-stepped. In order to maximize LC-SPM speed and minimize scattering losses, the device should be as thin as possible, which means removing the 2π degeneracies from the phase profile. That step produces phase "resets" in the final stair-stepped phase profile.

It is already known that these resets do carry a penalty, but prior analyses considered only the case in which individual stair-step approximated blaze periods contain fixed and identical numbers of segments. This limits the use of segmented liquid crystal devices to a finite number of discretely separated steering angles. That result has been extended to the more general case of phase resets falling on, and not just between, electrode segments. There is a correct choice for the phase value to be produced at electrodes for which a reset falls within bounds of that electrode. If the phase stair-step is obtained by averaging the value of the underlying blazed phase profile over each electrode before removing the 2π degeneracy, analysis shows that it does

not matter where the reset falls. As a result, we can say that continuous beam steering is possible without any added penalty.

As is already known, increasing the steering angle (i.e. blazes of smaller size) or increasing the number of waves being corrected by a given fixed aperture results in increased diffractive losses. Use of eight steps per blaze will result in theoretical 5% loss, measured at receiver's collecting aperture.

This limiting behavior occurs when the electrode size/spacing is much larger than either a wavelength of light, or than the spatial extent of liquid crystal elasticity or fringing fields produced by the finiteness of electrodes. Those other limiting behaviors will be the subject of future study.

Appendix A

As has been done in other studies[8,9,15], simply periodic liquid crystal phase gratings such as shown in Fig. 3a can be approached as a linear system[16], making the task of Fourier analysis straightforward. Here, we will also apply that approach to the grating represented in Fig. 11b. Making use of the thin-layer approximation, the transmission function of the grating is:

$$f(x)=\left(\left\{\left[\exp\left(i2\pi\, x/a\right)\sum_{n=-\infty}^{\infty}\delta(x-nw)\right]\otimes W(w)\right\}W(L)\right)\otimes\sum_{m=-\infty}^{\infty}\delta(x-mL) \tag{6}$$

$$W(w)=rect\left(\frac{x-w/2}{w}\right) \tag{7}$$

$$W(L)=rect\left(\frac{x-L/2}{L}\right) \tag{8}$$

where the exponential is the ideal linear phase ramp (which this grating is to approximate), sampled once for each stair-step of width w in the device using the first impulse function series. Each sampled phase value is then ascribed uniformly to its entire stair-step width (i.e. electrode spacing in an LC-SPM) by convolving the sampled phase with a window of the same width. This produces an infinite stair-stepped phase function. The stair-step is truncated by the period L over which the stair-step representation repeats. In general, L is not necessarily equal to a, but is always *some* integer multiple of a. This repeatable grating unit (distance between identically stair-stepped "blazes") is then reproduced infinitely by the last convolution.

The reader may note that this is an infinite grating, i.e. the function above is not windowed with a finite aperture. The above infinite form will produce a diffraction pattern nearly identical to the pattern resulting from an aperture large enough to avoid "significant"

truncation of a Gaussian beam passing through it. In other words, this is the appropriate expression of surface fields emerging from an optical communication transmitter such as described in the body of this paper.

The Fraunhofer diffraction approximation can be obtained from Eq. (6) above by calculating the Fourier transform of each of it parts, and then composing the composite result assuming a linear system. The resulting diffraction profile is:

$$F(u) = \sum_{n=-\infty}^{\infty} \mathrm{sinc}\left[\frac{w}{2}(nu_w + u_a)\right] \mathrm{sinc}\left[\frac{L}{2}(u - nu_w - u_a)\right] \tag{9}$$

$$u_a = \frac{2\pi}{a} \tag{10}$$

$$u_w = \frac{2\pi}{w} \tag{11}$$

where u_a and u_w are spatial frequencies characteristic of the pre-segmented distances between resets and the electrode spacing, a and w, respectively. The last impulse function series in Eq. (6) restricts the permissible spatial frequencies u to:

$$u = \frac{2\pi m}{L} \tag{12}$$

where L is the periodic length of the stair-stepped grating's phase profile (which may include any number of stepped "blazes"), and m is an integer. The spatial frequency can be converted to a far field angle from the relation $u=k\sin(\theta)$.

Calculations using Eq. (9) agree with the results shown in Fig. 11 for the case in which all electrodes (including those overlapping reset edges) are assigned a phase equal to the average of the desired linear phase ramp, then operated on by-modulo-2π.

References

1. K. Wilson, "Optical Communications for Deep Space Missions", IEEE Communications **38**, 8, 134-139, (2000).
2. C. D. Edwards, C. T. Stelzried, L. J. Deutsch, L. Swanson, "NASA's Deep-Space Telecommunications Road Map", TMO Progress Report **42-136**, Jet Propulsion Laboratory, Pasadena CA, 1-20, (1999).
3. C. Chen, J. W. Alexander, H. Hemmati, S. Monacos, T. Yan, S. Lee, J. R. Lesh, S. Zingales, "System Requirements for a Deep Space Optical Transceiver", SPIE Proc. **3615**, 142-152, (1999).
4. H. Hemmati, K. Wilson, M. Sue, L. Harcke, M. Wilhelm, C. Chen, J. Lesh, Y. Feria, "Comparative Study of Optical and Radio-Frequency Communication Systems for a Deep-Space Mission", TDA Progress Report **42-128**, Jet Propulsion Laboratory, Pasadena CA, 1-33, (1997).
5. S. Lee, J. W. Alexander, G. G. Ortiz, "Sub-Microradian Pointing System Design for Deep-Space Optical Communication", in *Free-Space Laser Communication Technologies XIII*, G. Stephen Mecherle, ed., Proc. SPIE **4272**, 104-111 (2001).
6. J. W. Alexander, S. Lee, C. Chen, "Pointing and Tracking Concepts for Deep Space Missions", in *Free-Space Laser Communication Technologies XI*, G. Stephen Mecherle, ed., Proc. SPIE **3615**, 230-249 (1999).
7. A. Gibson, "Laser Pointing Technology", in *Laser Weapons Technology*, T.D. Steiner and P. H. Merritt, eds., Proc. SPIE **4034**, 165-174 (2000).

8. P. F. McManamon, T. A. Dorschner, D. L. Corkum, L. J. Friedman, D. S. Hobbs, M. Holz, S. Lieberman, H. Q. Nguyen, D. P. Resler, R. C. Sharp, and E. A. Watson, "Optical Phased Array Technology", Proc. of the IEEE **84**, 268-297 (1996).

9. E. A. Watson, P. F. McManamon, L. J. Barnes, and A. J. Carney, "Application of Dynamic Gratings to Broad Spectral Band Beam Steering", in *Laser Beam Propagation and Control*, H. Weichel and L. F. Desandre, eds., Proc. SPIE **2120**, 178-185 (1994).

10. D. P. Resler, D. S. Hobbs, R.C. Sharp, L. J. Friedman, T. A. Dorschner, "High-Efficiency Liquid-Crystal Optical Phased-Array Beam Steering", Opt. Lett. **21**, 689-691, (1996).

11. M. T. Gruneisen, T. Martinez, D. L. Lubin, "Dynamic Holography for High-Dynamic-Range Two-Dimensional Laser Wavefront Control", in *High-Resolution Wavefront Control: Methods, Devices, and Applications III*, J. D. Gonglewski, M. A. Vorontsov, and M. T. Gruneisen, eds., Proc. SPIE **4493**, High-Resolution Wavefront Control: Methods, Devices, and Applications, San Diego, CA., Aug. 1-3 (2001).

12. M. Born and E. Wolf, *Principles of Optics*, 6th Edition (Cambridge University Press, Cambridge 1997).

13. C. M. Titus, *Refractive and Diffractive Liquid Crystal Beam Steering Devices*, Kent State Univ. Dissertation (2000).

14. J. D. Zook, "Light Beam Deflector Performance: a Comparative Analysis", Appl. Opt. **13**, 875-887 (1974).

15. V. Dominic, A. Carney, and E. Watson, "Measurement and Modeling of the Angular Dispersion in Liquid Crystal Broadband Beam Steering Devices", Opt. Eng. **35**, 3371-3379 (1996).

16. J. W. Goodman, *Introduction to Fourier Optics*, (McGraw-Hill, New York 1968).

Figure Captions

Figure 1. Conception of three periods from a liquid crystal spatial phase modulator, with lower electrode voltages selected to produce blazed-phase grating.

Figure 2. Ideal linear phase ramp, characteristic of deflected plane waves, has its 2π phase degeneracies removed.

Figure 3. Phase retardation profiles produced by (a) Large Pixel OPA showing phase stair-stepping, and (b) Small Pixel OPA, showing evidence of "phase smoothing" resulting from increased significance of the spatial extent of fringing fields and liquid crystal elasticity

Figure 4. Intensity profiles, in the far field, of a Gaussian beam which has been truncated in the plane of the minimum waist. Intensity is normalized to that of an unhindered beam. At the beam center, this ratio is the Strehl ratio.

Figure 5. Effect of sinusoidal surface undulations on far field intensity distribution of Gaussian beam reflected from a non-ideal mirror surface. . At the beam center, this ratio is the Strehl ratio.

Figure 6. Strehl ratio vs. surface undulation amplitude, for 3 different undulation spatial frequencies, for a Gaussian beam reflected from anon-ideal mirror surface.

Figure 7. Coverage of far field, from an OPA for which steering resolution is limited to the spot resolution. Not all parts of far field will be able to see the signal at its most intense.

Figure 8. Ideal linear phase ramp, after application of modulo-2π operation, overlaid onto patterned electrodes, for the case in which phase resets do not coincide with the boundary between electrodes.

Figure 9. For the case of Figure 7, applying the phase-averaging operation to the interperiod electrode, after first applying the modulo-2π operation to the ideal linear phase ramp.

Figure 10. For the case of Figure 7, applying the modulo-2π operation to the interperiod electrode, after first applying the phase-averaging operation to the ideal linear phase ramp.

Figure 11. Sections of grating phase profile, after (a) application of modulo-2π and then phase-averaging operation, and (b) reversing the order of those operations.

Figure 12. Strehl ratio vs. number of electrodes per ideal blaze period, showing the effects of non-integer numbers for the two methods of assigning phase to interperiod electrodes.

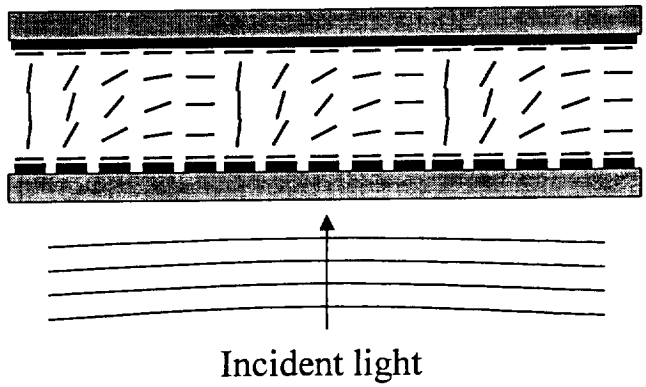

Figure 1. Conception of three periods from a liquid crystal spatial phase modulator, with lower electrode voltages selected to produce blazed-phase grating.

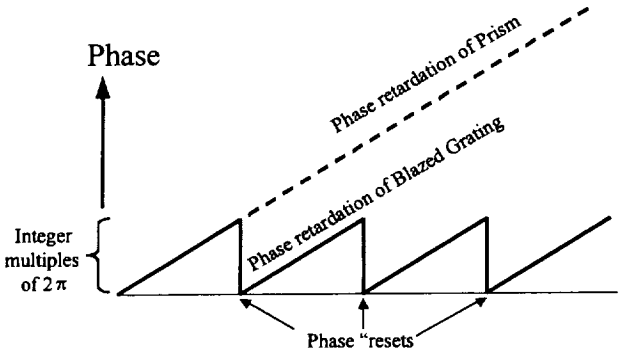

Figure 2. Ideal linear phase ramp, characteristic of deflected plane waves, has its 2π phase degeneracies removed.

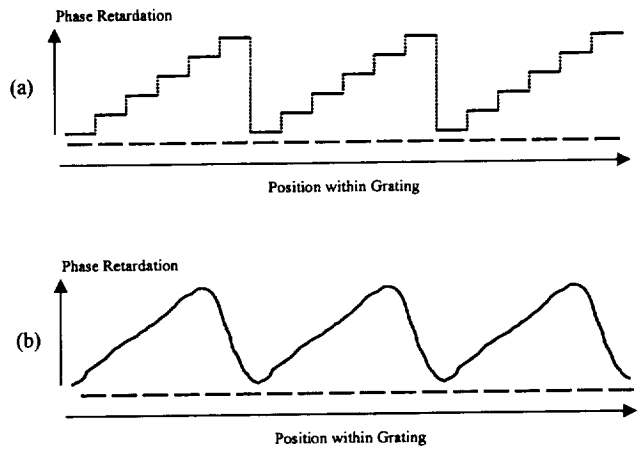

Figure 3. Phase retardation profiles produced by (a) Large Pixel OPA showing phase stair-stepping, and (b) Small Pixel OPA, showing evidence of "phase smoothing" resulting from increased significance of the spatial extent of fringing fields and liquid crystal elasticity

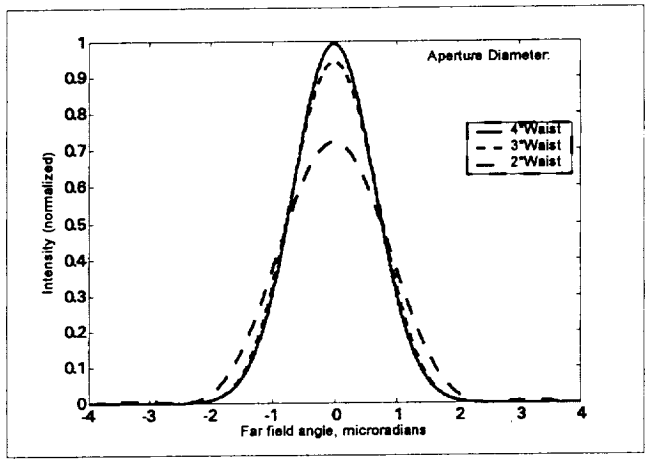

Figure 4. Intensity profiles, in the far field, of a Gaussian beam which has been truncated in the plane of the minimum waist. Intensity is normalized to that of an unhindered beam. At the beam center, this ratio is the Strehl ratio.

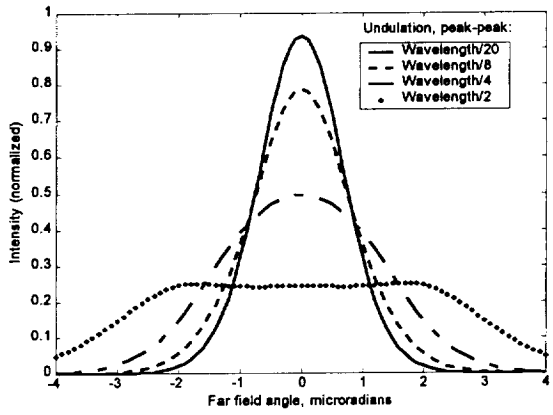

Figure 5. Effect of sinusoidal surface undulations on far field intensity distribution of Gaussian beam reflected from a non-ideal mirror surface. . At the beam center, this ratio is the Strehl ratio.

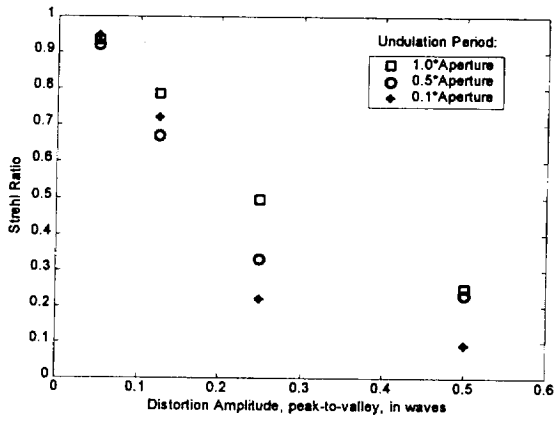

Figure 6. Strehl ratio vs. surface undulation amplitude, for 3 different undulation spatial frequencies, for a Gaussian beam reflected from anon-ideal mirror surface.

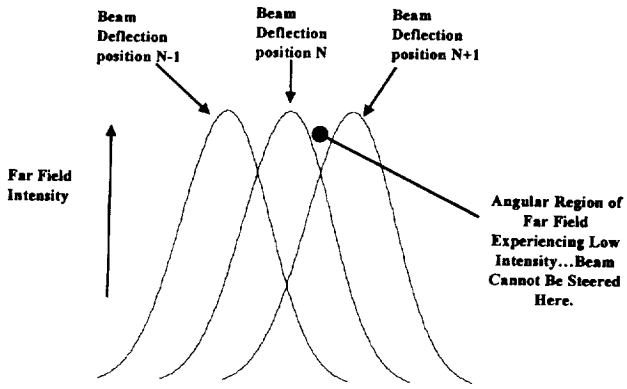

Figure 7. Coverage of far field, from an OPA for which steering resolution is limited to the spot resolution. Not all parts of far field will be able to see the signal at its most intense.

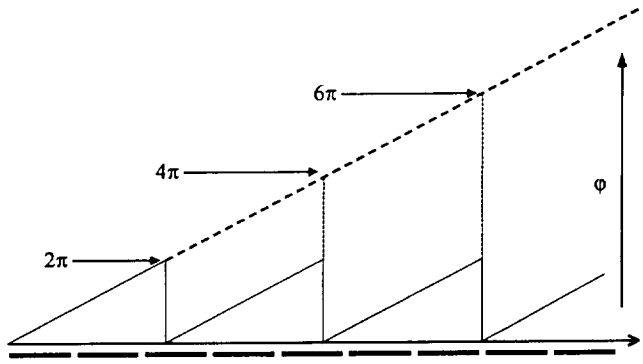

Figure 8. Ideal linear phase ramp, after application of modulo-2π operation, overlaid onto patterned electrodes, for the case in which phase resets do not coincide with the boundary between electrodes.

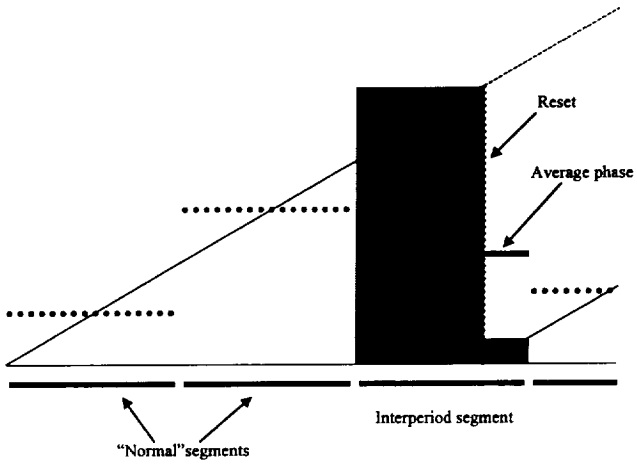

Figure 9. For the case of Figure 7, applying the phase-averaging operation to the interperiod electrode, after first applying the modulo-2π operation to the ideal linear phase ramp.

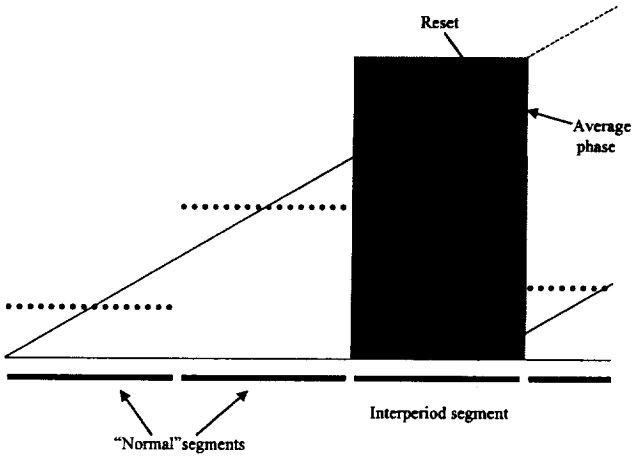

Figure 10. For the case of Figure 7, applying the modulo-2π operation to the interperiod electrode, after first applying the phase-averaging operation to the ideal linear phase ramp.

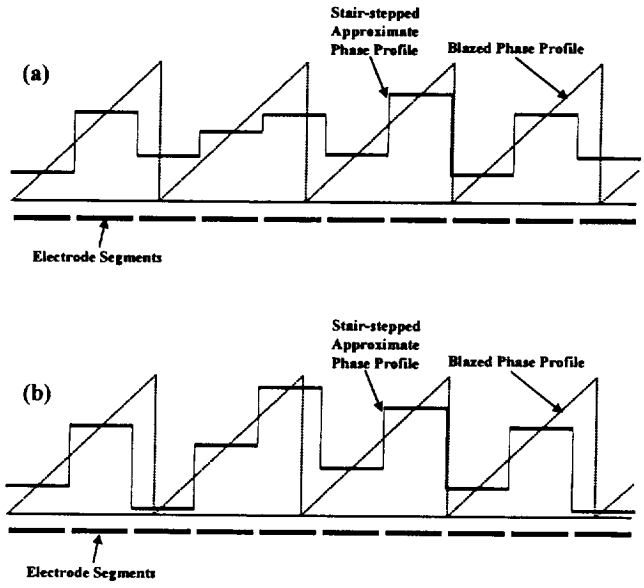

Figure 11. Sections of grating phase profile, after (a) application of modulo-2π and then phase-averaging operation, and (b) reversing the order of those operations.

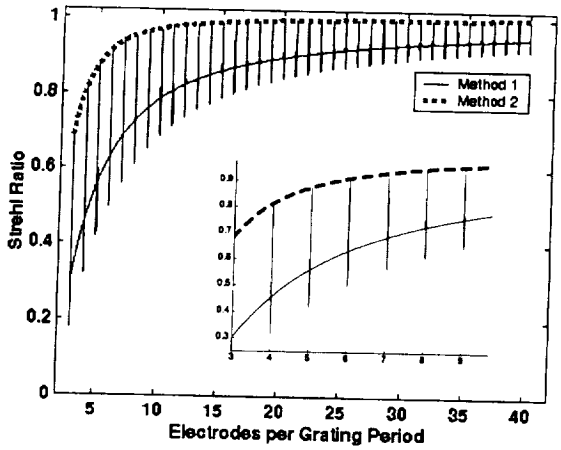

Figure 12. Strehl ratio vs. number of electrodes per ideal blaze period, showing the effects of non-integer numbers for the two methods of assigning phase to interperiod electrodes.